The Virtual Quantum Optics Laboratory

Brian R. La Cour, Maria Maynard, Parth Shroff, Gabriel Ko, and Evan Ellis
Applied Research Laboratories
The University of Texas at Austin
Austin, TX, USA
blacour@arlut.utexas.edu

***Abstract*—We present a web-based software tool, the Virtual Quantum Optics Laboratory (VQOL), that may be used for designing and executing realistic simulations of quantum optics experiments. A graphical user interface allows one to rapidly build and configure a variety of different optical experiments, while the runtime environment provides unique capabilities for visualization and analysis. All standard linear optical components are available as well as sources of thermal, coherent, and entangled Gaussian states. A unique aspect of VQOL is the introduction of non-Gaussian measurements using detectors modeled as deterministic devices that "click" when the amplitude of the light falls above a given threshold. We describe the underlying theoretical models and provide some illustrative examples. We find that VQOL provides a faithful representation of many experimental quantum optics phenomena and may serve as both a useful instructional tool for students as well as a valuable research tool for practitioners.**

***Index Terms*—quantum, optics, simulation, experiments, education**

I. Introduction

The subject of quantum mechanics is notoriously difficult to understand and teach [1], [2]. In part, this stems from the complex mathematics often required to describe quantum systems, but the many conceptual difficulties of the subject pose what is arguably an even greater challenge. Ideally, one would go to the laboratory and discover quantum phenomena first hand, but this is not practical. A potential remedy is to use high-fidelity simulation tools with which one may explore the quantum world. Such an approach can indeed be of great practical and pedagogical benefit, but simulators must strike the right balance between simplicity and realism while giving users ample freedom to explore. Simulations that are overly idealized or abstract may rob one of the deep insights that may be gained when working with real experiments.

The choice of physical systems is also of great importance. We believe the physics of *light* provides an excellent approach with which to introduce and study quantum concepts. In using light, one can take advantage of the many classical concepts that translate directly to their quantum counterparts. The polarization of classical light, for example, provides a direct analogy (*sans* normalization) to a photon polarization state, which is itself one particular representation of a quantum bit or *qubit*. Furthermore, classical linear optical devices, such as beam splitters, phase shifters, wave plates, etc., translate directly to general unitary transformations. Even nonlinear optical phenomena, such as parametric down conversion, can be introduced in classical terms.

The one important point of departure in these analogies lies in measurement. Classical Gaussian measurements of light are typically in the form of time-varying intensities, but quantum light may also be measured as non-Gaussian detection events or "clicks" of, say, an avalanche photodiode. Although quantum phenomena can certainly be found in intensity measures, as is done in heterodyne and homodyne detection, discrete detection events are essential for exhibiting the particle-like behavior of light. Thus, the difference between these two types of measurements can be used to encapsulate the differences between classical and quantum light [3].

These considerations led us to develop a novel quantum optics simulation tool we call the Virtual Quantum Optics Laboratory (VQOL). VQOL is a unique marriage of classical and quantum optics based on two simple principles: First, we formally treat the vacuum modes of quantum optics as real (rather than virtual) random electromagnetic radiation corresponding to the zero-point field. Second, detectors are modeled as deterministic devices that "click" when the intensity of incident light, including contributions from the vacuum, falls above a user-defined threshold. These two ingredients have been shown to be capable of reproducing many of phenomena one observes in real quantum experiments [4], [5], [6].

There are, of course, a plethora of existing resources for simulating quantum optics, ranging from pedagogical games to sophisticated research tools [7], [8], [9]. We shall highlight a few that we believe are particularly relevant and contrast them with VQOL.

The first is Strawberry Fields by Xanadu, an open-source programming architecture for simulating continuous-variable photonic quantum computers [10]. Simulator backends allow users to construct quantum states through a sequence of unitary gates and apply both Gaussian (e.g., homodyne) and non-Gaussian (e.g., photon counting) measurements. VQOL is similar to Strawberry Fields in using only Gaussian states, either thermal, coherent, or entangled, as light sources. It differs in its focus on experimental design, vice abstract gate operations, and in treating detectors as nonideal devices.

QuantumLab by the University of Erlangen-Nuremberg is a web-based resource that uses Adobe Flash-Player to illustrate various real-world quantum optics experiments [11]. The experiments are performed in a real laboratory and conducted under various configurations and parameter settings. Users can select from among these options and visualize the real (not simulated) data that were actually observed. QuantumLab is an

excellent resource for demonstrating real-world quantum optics phenomena, but it lacks the flexibility provided by VQOL to allow users to design and conduct their own experiments.

Finally, Quantum Lab by Quantum Flytrap is a colorful web-based tool that allows users to design and run their own custom optics experiments [12], [13]. A virtual optics table with a drag-and-drop pallette of components allows users to design and run a variety of optical experiments. Lasers are modeled as simple, on-demand single-photon sources, while non-linear crystals provide a source of idealized entangled photon pairs. Detectors are treated as having perfect efficiency and no dark counts, with random detection events that strictly follow the Born rule. Quantum Lab is similar to VQOL in providing an open-ended user interface to design and conduct experiments. VQOL differs, however, in its use of more realistic light sources and non-ideal detectors. The advantage of our approach, we believe, lies in its ability to provide a more faithful representation of what is actually observed.

With these preliminary considerations, we summarize the organization of the paper as follows. In Section II we provide a brief description of the VQOL software from a user interface perspective. Sections III and IV discusses the modeling assumptions and component descriptions underlying VQOL, with particular emphasis on departures from standard classical optics necessitated by our explicit use of vacuum modes. Section V gives some examples of experiments that may be performed with VQOL. We discuss the pedagogical and research applications in Section VI and summarize our conclusions in Section VII.

II. Software Description

This paper describes version 1.0 of the Virtual Quantum Optics Laboratory. VQOL may be used online via the universal resource locator (URL) `https://www.vqol.org`. Simulations are run locally on the user's device using JavaScript. Using either a text editor or graphical interface, the user may define an experiment by placing (and optionally orienting, and configuring) various component devices on a gridded virtual optics table. Figure 1 illustrates the interface and shows an implementation of a quantum teleportation experiment. Sample experiments are provided, but the user is free (and encouraged) to design their own.

Since polarization figures heavily in many quantum optics experiments, a design decision was made to use color to represent polarization. Although the use of color to represent polarization can be misleading, as it should properly be construed as indicating wavelength (or frequency), we have found this causes no great confusion and is preferably to a two-dimensional projection of the electric field, which may be visually ambiguous. The six main polarization states (and corresponding colors) are horizontal (red), vertical (blue), diagonal (yellow), anti-diagonal (green), right circular (orange), and left circular (violet). Other, general elliptical polarizations are show in a color that is a blend of these six. An illustration of these various colors, as seen on the Bloch sphere (or, equivalently, the Poincaré sphere) is given in Fig. 2. For this

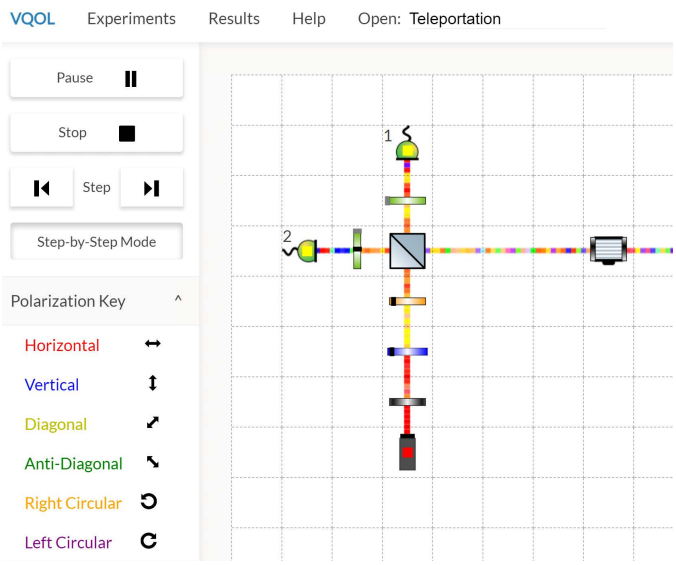

Fig. 1. (Color online) VQOL quantum teleportation experiment. Colors indicate different polarization states, as indicated in the Polarization Key.

choice of colors, individuals with partially impaired color perception will generally be able to distinguish one of two orthogonal polarizations but may have difficulty distinguishing between non-orthogonal polarizations.

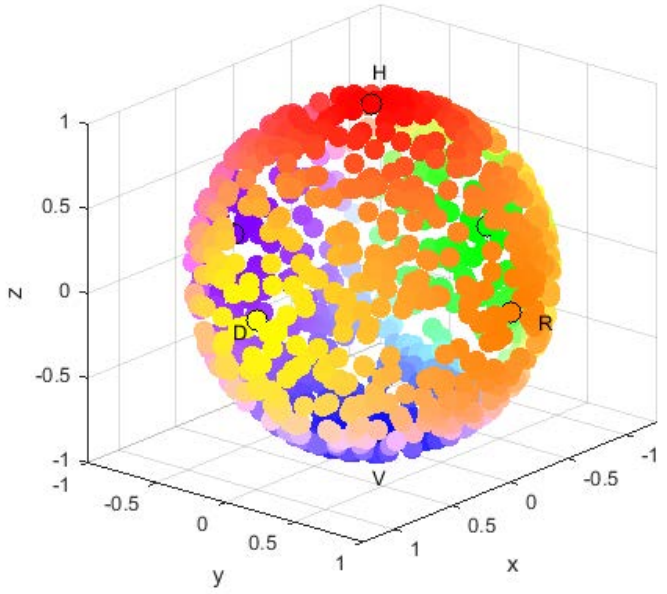

Fig. 2. (Color online) Colors used by VQOL for various polarization states, as represented on the Bloch sphere.

Control buttons allow the user to start, pause, or stop the experiment. There are also options to run the experiment in slow motion, step forward, or step back. (Stepping back and then forward produces the same outcome.) Experiments run for a default time of 1 ms (in simulation time, not real time), but this may be changed in the graphical interface or by editing the variable `num_seconds`. VQOL operates in time segments of

$\Delta t = 1\,\mu$s, so the default time of 1 ms corresponds to 1000 time samples. The actual runtime of an experiment will depend on the local machine and the complexity of the experiment; a 1-ms experiment typically runs in about 15 s of real time. Setting the time to exactly $1\,\mu$s gives something that *looks* like a single photon, though this is not how VQOL actually models quantum light.

A sample experiment for measuring the power of light passing through a polarizer rotated 30° is the following:

```
# Malus's law experiment
num_seconds = 1e-3
offline_mode = False
Laser, x=1, y=1, orientation=0
Polarizer, x=3, y=1, orientation=0, angle=30
PowerMeter, x=5, y=1
```

Note that comments may be added within the experiment using the hash symbol (#).

The optional variable `offline_mode` may be used to control the graphics display. By default, this variable is set to `False`. If set to `True`, VQOL will run the simulation without producing any animation graphics. This can be useful for doing long simulations in which the user only wants the final results of the experiment, as it will generally run much faster. In either case, once the experiment is completed the results are displayed on the screen and stored in a comma separated value (csv) file for later analysis.

One may use JavaScript directly within the web-based editor to automate the simulation of multiple experimental scenarios. To initiate the interpreter, the experiment editor should begin with `<JS>`. An example for an experiment investigating Malus's law is shown below.

```
<JS>
// Malus's law experiment
for (let theta=0; theta<=90; theta+=5){
  runSimulation(
  "num_seconds = 1e-6\n" +
  "Laser, x=1, y=1, orientation=0\n" +
  "Polarizer, x = 3, y=1, orientation=0," +
  " angle=" + theta + "\n" +
  "PowerMeter, x=5, y=1"
  )
}
```

The script runs 19 separate experiments, each 1-μs in duration, with polarizer angles of $0°, 5°, \ldots, 90°$. The "`//`" symbol indicates a single-line comment, the "+" symbols perform string concatenation, and the "`\n`" symbol implements a newline character. The results are stored in a set of folders that may be downloaded as a single ZIP-formatted file.

III. Model Description

In VQOL, light may travel in only one of four directions in the plane of the optics table: right (→), left (←), up (↑), and down (↓). Out-of-plane or non-rectilinear directions are currently not supported. Each Δt time segment has a polarization given by a dimensionless Jones vector of the form

$$\boldsymbol{a} = \begin{pmatrix} a_H \\ a_V \end{pmatrix} , \tag{1}$$

where a_H and a_V are the complex horizontal and vertical polarization components, respectively.

For monochromatic light traveling, say, to the right with Jones vector $\boldsymbol{a}$, the electric field at the coordinate (x, y) and time t is given by

$$\boldsymbol{E}(x, y, t) \propto -(a_H \hat{\boldsymbol{y}} + a_V \hat{\boldsymbol{z}})\, \mathrm{e}^{\mathrm{i}(kx - \omega t)} + \text{c.c.} , \tag{2}$$

where ω is the angular frequency of the light, $k = \omega/c$ is the wavenumber, c is the speed of light in a vacuum, and "c.c." denotes the complex conjugate of the term to the left. Note that VQOL uses a right-handed coordinate system such that the upper left corner is the origin, $\hat{\boldsymbol{x}}$ points to the right, $\hat{\boldsymbol{y}}$ points down, and $\hat{\boldsymbol{z}}$ points into the optics table.

Classically, the Jones vector of the vacuum is simply the zero vector. Quantum mechanically, we describe the vacuum by the Fock state $|0\rangle_H \otimes |0\rangle_V$, where $|0\rangle_H$ and $|0\rangle_V$ are the vacuum states of the horizontal and vertical polarization modes, respectively, and $\otimes$ denotes the tensor product. More generally, the Wigner function of a thermal state for a given wave vector mode is given by

$$W_T(a_H, a_V) = \frac{1}{\pi^2 \sigma_T^4} \exp\left(-\frac{|a_H|^2 + |a_V|^2}{\sigma_T^2} \right) , \tag{3}$$

where $\sigma_T > 0$ is given by Planck's second theory of black body radiation. Specifically,

$$\sigma_T^2 = \frac{1}{\mathrm{e}^{\hbar\omega/(k_\mathrm{B} T)} - 1} + \frac{1}{2} , \tag{4}$$

where T is the absolute temperature (in Kelvin), k_B is Boltzmann's constant, and $\hbar$ is Planck's constant (divided by 2π). For $T = 0$, we define $\sigma_0^2 = 1/2$ as the limit of σ_T^2 as $T \to 0$. At optical wavelengths and room temperature, $\sigma_T \approx \sigma_0$, which is taken to be the default in VQOL. In quantum mechanical terms, $\sigma_T^2 \hbar\omega$ is the modal energy for a given wave vector and polarization, so each vacuum mode has an associated modal energy of $\frac{1}{2}\hbar\omega$.

In VQOL, a vacuum state is treated as having a random Jones vector of the form $\sigma_0 \boldsymbol{z}$, where

$$\boldsymbol{z} = \begin{pmatrix} z_H \\ z_V \end{pmatrix} \tag{5}$$

is a standard complex Gaussian random vector, for which z_H and z_V are independent standard complex Gaussian random variables. (We say that z is a standard complex Gaussian random variable if $\mathsf{E}[z] = 0$, $\mathsf{E}[z^2] = 0$, and $\mathsf{E}[|z|^2] = 1$, where $\mathsf{E}[\cdot]$ denotes the expectation value of a random variable.) The probability density function of the Jones vector is therefore identical to the Wigner function of the vacuum state, by the optical equivalence theorem [14]. Note that each vacuum mode has a random modal energy that is exponentially distributed with a mean value of $\frac{1}{2}\hbar\omega$. Vacuum modes are assumed to be coherent (i.e., constant) over the time interval Δt but are independent from one time step to the next.

In classical optics, a monochromatic plane wave may be represented by the Jones vector

$$\boldsymbol{\alpha} = \begin{pmatrix} \alpha_H \\ \alpha_V \end{pmatrix} , \tag{6}$$

where α_H and α_V are complex numbers specifying the amplitude and phase of the horizontal and vertical polarization components. Similarly, in quantum optics a monochromatic plane wave is described by the separable coherent state $|\alpha_H\rangle \otimes |\alpha_V\rangle$. In VQOL, a mathematically equivalent representation is obtained by simply adding the vacuum components, resulting in the Jones vector

$$\boldsymbol{a} = \boldsymbol{\alpha} + \sigma_0 \boldsymbol{v} = \begin{pmatrix} \alpha_H + \sigma_0 z_H \\ \alpha_V + \sigma_0 z_V \end{pmatrix} . \tag{7}$$

This, then, provides a model for laser light that includes classical light as a limiting case when the vacuum fluctuations can be neglected.

VQOL also provides a source of entangled light, modeled as a pair of random Jones vectors whose joint probability density function is identical to the Wigner function of a multi-mode Gaussian squeezed vacuum state. The random vectors are defined in terms of a pair of random vectors in a manner described in Sec. IV and, more generally, in Ref. [5].

The ability to model coherent and squeezed vacuum states as complex Gaussian random variables follows directly from the Gaussian nature of the quantum states themselves. In this sense, they may be deemed classical. (We note, however, that entangled Gaussian states need not admit a positive Glauber-Sudarshan P function representation and, in this sense, may be deemed non-classical.) Non-Gaussian measurements are therefore essential to provide a mechanism for observing nonclassical behavior, and these are provided by threshold detectors, which we shall now describe.

In VQOL we model detectors as devices that produce a detection event (or "click") when the amplitude of either the horizontal or vertical mode falls above a given threshold $\gamma \geq 0$. Thus, a detection corresponds to the event

$$D = \left\{ |a_H| > \gamma \quad \text{or} \quad |a_V| > \gamma \right\} . \tag{8}$$

This particular definition of a detection event was chosen for its mathematical simplicity. Using instead the magnitude of the Jones vector may be more physically motivated but would yield similar results.

For coherent light, the probability of event D occurring is given by

$$\Pr[D] = 1 - P_{\gamma,\sigma_0}(\alpha_H)\, P_{\gamma,\sigma_0}(\alpha_V) , \tag{9}$$

where

$$P_{\gamma,\sigma}(\alpha) = 1 - Q_1(\sqrt{2}|\alpha|/\sigma, \sqrt{2}\gamma/\sigma) \tag{10}$$

and $Q_1(\cdot,\cdot)$ is the Marcum Q function [15]. As we shall see, this result is different from the quantum probability of $1 - \exp(-|\alpha_H|^2 - |\alpha_V|^2)$ associated with one or more photons in a coherent state, as our model *implicitly* incorporates the non-idealities of dark counts and sub-unity detection efficiency.

To see this, note that we may approximate $P_{\gamma,\sigma}(\alpha)$, to second order in $|\alpha|$ and γ, as

$$P_{\gamma,\sigma}(\alpha) = 1 - \mathrm{e}^{-\gamma^2/\sigma^2} \left[1 + \frac{\gamma^2}{\sigma^4} |\alpha|^2 + \mathcal{O}(|\alpha|^4) \right] . \tag{11}$$

Thus, to lowest order,

$$\Pr[D] \approx \delta + \eta \left(|\alpha_H|^2 + |\alpha_V|^2 \right) , \tag{12}$$

where

$$\delta = 1 - \left(1 - \mathrm{e}^{-\gamma^2/\sigma_0^2} \right)^2 \tag{13}$$

is the probability of a dark count and

$$\eta = \mathrm{e}^{-\gamma^2/\sigma_0^2} \left(1 - \mathrm{e}^{-\gamma^2/\sigma_0^2} \right) \frac{\gamma^2}{\sigma_0^4} \tag{14}$$

is the nominal detection efficiency. In this way we can see that VQOL reproduces the Born rule in the limit of weak coherent light (for fixed γ) and under the non-ideal, albeit realistic, conditions of a nonzero dark count rate and imperfect detection efficiency. Note that it is not possible within the above parameterization to achieve both an arbitrarily low dark count rate and a detection efficiency arbitrarily close to one. However, using an operational definition of detection efficiency, it is possible to achieve an arbitrarily good detection efficiency for a given dark count rate, as described in Sec. V-A.

IV. Description of Components

A. Passive Optical Components

In VQOL, lossless optical components behave in accordance with their classical Jones matrix description. For example, the action of a **half-wave plate (HWP)** with a fast-axis angle of θ is described by the Jones matrix

$$\mathsf{HWP}(\theta) = \begin{bmatrix} \cos(2\theta) & \sin(2\theta) \\ \sin(2\theta) & -\cos(2\theta) \end{bmatrix} . \tag{15}$$

The angle θ is measured counterclockwise from the horizontal. (Figure 3 provides a graphical illustration.)

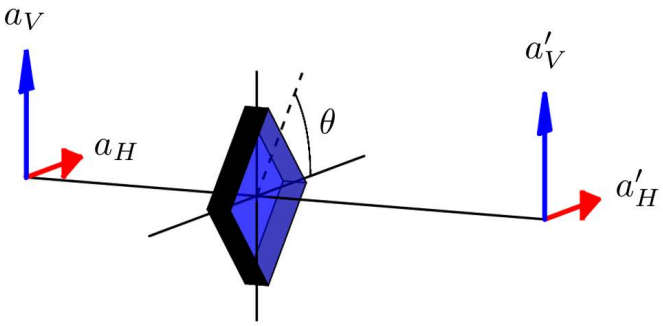

Fig. 3. (Color online) Graphical illustration of the action of a wave plate with a fast-axis angle of θ. The input $(a_H, a_V)^{\mathsf{T}}$ is shown on the left, while the output $(a'_H, a'_V)^{\mathsf{T}}$ is shown on the right.

Similarly, a **quarter-wave plate (QWP)** with a fast-axis angle of θ has the Jones matrix

$$\mathsf{QWP}(\theta) = \begin{bmatrix} \cos^2\theta + \mathrm{i}\sin^2\theta & (1-\mathrm{i})\cos\theta\sin\theta \\ (1-\mathrm{i})\cos\theta\sin\theta & \sin^2\theta + \mathrm{i}\cos^2\theta \end{bmatrix} . \tag{16}$$

Finally, a **phase delay (PD)** component may be used to apply a common phase shift $\mathrm{e}^{\mathrm{i}\phi}$ to both components. This is represented by the Jones matrix

$$\mathsf{PD}(\phi) = \begin{bmatrix} \mathrm{e}^{\mathrm{i}\phi} & 0 \\ 0 & \mathrm{e}^{\mathrm{i}\phi} \end{bmatrix} . \tag{17}$$

The related **dephaser (DPH)** component is treated as a phase delay for which ϕ is a random variable that is uniformly distributed on the interval $[0, 2\pi]$ and generated independently at each time step.

For longer delays, a **time delay (TD)** component may be used. This component delays the light beam by an integer number of time steps, in units of Δt. The default is zero (no delay). A delay of 10 will set the light beam back by one whole grid space. Physically, a time delay may be implemented with a coil of optical fiber, although in VQOL the time delay component is both amplitude and polarization preserving.

VQOL also offers the more general **rotator (R)** and **phase retarder (PR)** components, whose Jones matrices are

$$\mathsf{R}(\theta) = \begin{bmatrix} \cos\theta & -\sin\theta \\ \sin\theta & \cos\theta \end{bmatrix} , \tag{18}$$

for $\theta \in [0°, 90°]$, and

$$\mathsf{PR}(\phi) = \begin{bmatrix} 1 & 0 \\ 0 & \mathrm{e}^{\mathrm{i}\phi} \end{bmatrix} , \tag{19}$$

respectively.

A general unitary may be represented by a rotator, two phase retarders, and a phase delay as follows: [16], [17]

$$\mathsf{U}(\chi, \phi, \theta, \lambda) = \mathsf{PD}(\chi)\, \mathsf{PR}(\phi)\, \mathsf{R}(\theta)\, \mathsf{PR}(\lambda) . \tag{20}$$

Taking $\theta = \frac{1}{2}\cos^{-1}(2u-1)$, where u is uniformly distributed on the interval $[0, 1]$, and taking ϕ, λ, χ to be independent and uniformly distributed on the interval $[0, 2\pi]$, the matrix $\mathsf{U}(\chi, \phi, \theta, \lambda)$ becomes a Haar-distributed random matrix. This is used to define a **depolarizer (DP)** in VQOL as a component that applies a random $\mathsf{U}(\chi, \phi, \theta, \lambda)$ at each time step.

Lossy components are treated differently in VQOL from their classical counterparts. In quantum optics, attenuation may be treated as a partially transmitting beam splitter, where the second input port receives a vacuum mode. Similarly, in VQOL a **neutral density filter (NDF)** with, say, an optical density of $d \geq 0$ acting on a Jones vector $\boldsymbol{a} = (a_H, a_V)^{\mathsf{T}}$ has the following output:

$$\begin{pmatrix} a'_H \\ a'_V \end{pmatrix} = 10^{-d/2} \begin{pmatrix} a_H \\ a_V \end{pmatrix} + \left(1 - 10^{-d/2}\right) \sigma_0 \boldsymbol{z} , \tag{21}$$

where $\boldsymbol{z}$ is, again, an independent standard complex Gaussian random vector. VQOL also offers a **beam blocker (BB)** component, which transforms an input Jones vector $\boldsymbol{a}$ into a vacuum state $\sigma_0 \boldsymbol{z}$. This is equivalent to an NDF with $d \to \infty$.

In a similar manner, a general elliptical **polarizer (P)** acting on the Jones vector $\boldsymbol{a}$ has the following output:

$$\begin{pmatrix} a'_H \\ a'_V \end{pmatrix} = \mathsf{P}(\theta, \phi) \begin{pmatrix} a_H \\ a_V \end{pmatrix} + \Big[\mathbf{1} - \mathsf{P}(\theta, \phi)\Big] \sigma_0 \boldsymbol{z} , \tag{22}$$

where $\mathsf{P}(\theta, \phi)$ is the standard polarizer Jones matrix,

$$\mathsf{P}(\theta, \phi) = \begin{bmatrix} \cos^2\theta & \mathrm{e}^{-\mathrm{i}\phi}\cos\theta\sin\theta \\ \mathrm{e}^{\mathrm{i}\phi}\cos\theta\sin\theta & \sin^2\theta \end{bmatrix} , \tag{23}$$

and $\mathbf{1} - \mathsf{P}(\theta, \phi)$ is the complementary matrix projection. Note that the presence of an additional vacuum term in Eqn. (22) invalidates the *no-enhancement assumption* [18]. In other words, it is possible that $|a'_H|^2 + |a'_V|^2 > |a_H|^2 + |a_V|^2$ for a given instance of $\boldsymbol{z}$. This implies, in particular, that placing a polarizer in front of detector could generate a detection that, counterfactually, would not have occurred if the polarizer were not present!

A **beam splitter (BS)** in VQOL works much like a classical beam splitter. Given the input Jones vectors $\boldsymbol{a} = (a_H, a_V)^{\mathsf{T}}$ and $\boldsymbol{b} = (b_H, b_V)^{\mathsf{T}}$, the output is given by

$$\begin{pmatrix} a'_H \\ a'_V \\ b'_H \\ b'_V \end{pmatrix} = \begin{pmatrix} t & 0 & r & 0 \\ 0 & t & 0 & r \\ r & 0 & -t & 0 \\ 0 & r & 0 & -t \end{pmatrix} \begin{pmatrix} a_H \\ a_V \\ b_H \\ b_V \end{pmatrix} , \tag{24}$$

where $r \in [0, 1]$ is the reflection coefficient and $t = \sqrt{1 - r^2}$ is the transmission coefficient. (See Fig. 4.) A **mirror (M)** is a special case for which $r = 1$. Unitarity is maintained with the convention that a transmitted component has a minus sign applied to it when the corresponding reflection is to the left. Note that if a beam splitter is presented with only one input, the other is taken to be a pair of independent vacuum modes, represented by a random Jones vector $\sigma_0 \boldsymbol{z}$.

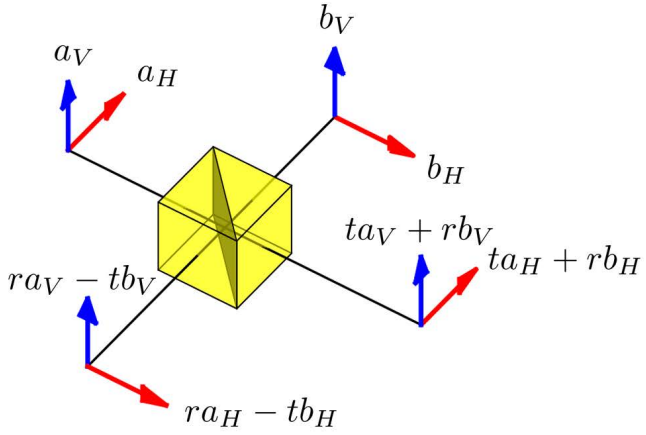

Fig. 4. (Color online) Graphical illustration of the action of a beam splitter with transmission (reflection) coefficient t (r). The inputs are shown in the upper left and right, while the outputs are shown in the lower left and right.

A **polarizing beam splitter (PBS)** works similarly to a regular beam splitter. Given two input Jones vectors, $\boldsymbol{a}$ and $\boldsymbol{b}$, the output is

$$\begin{pmatrix} a'_H \\ a'_V \\ b'_H \\ b'_V \end{pmatrix} = \begin{pmatrix} 1 & 0 & 0 & 0 \\ 0 & 0 & 0 & 1 \\ 0 & 0 & 1 & 0 \\ 0 & 1 & 0 & 0 \end{pmatrix} \begin{pmatrix} a_H \\ a_V \\ b_H \\ b_V \end{pmatrix} . \tag{25}$$

(See Fig. 5.) Again, if the PBS is presented with only one input, the other is taken to be a pair of independent vacuum modes. Consequently, the light exiting each output port need not be restricted to only horizontal or vertical polarization, as reflected components of the opposite polarization will contribute from the vacuum modes.

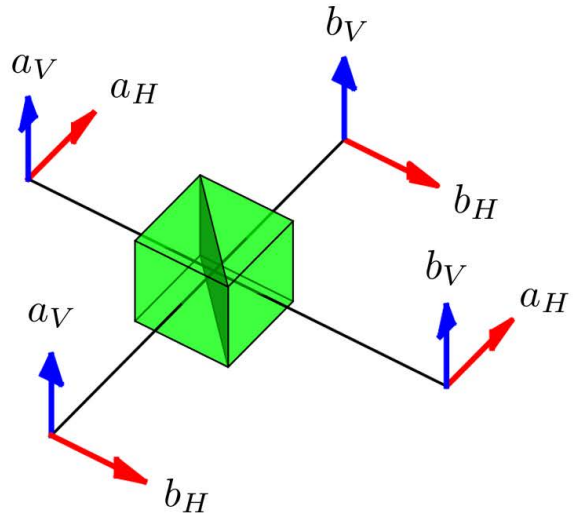

Fig. 5. (Color online) Graphical illustration of the action of a polarizing beam splitter. The inputs are in the upper left and right, while the outputs are in the lower left and right.

VQOL offers three PBS variants for different polarization bases. The default H/V basis transmits horizontal light and reflects vertical light, as described by Eqn. (25). An optional D/A basis transmits diagonal light and reflects anti-diagonal light, while the R/L basis option transmits right-circular light and reflects left-circular light. Specifically, if $\boldsymbol{a} = (a_H, a_V)^\mathsf{T}$ and $\boldsymbol{b} = (b_H, b_V)^\mathsf{T}$ are the Jones vectors for the inputs to a D/A-basis PBS, then the output Jones vectors are

$$\begin{pmatrix} a'_H \\ a'_V \end{pmatrix} = \frac{a_H + a_V}{2} \begin{pmatrix} 1 \\ 1 \end{pmatrix} + \frac{b_H - b_V}{2} \begin{pmatrix} 1 \\ -1 \end{pmatrix} \tag{26}$$

and

$$\begin{pmatrix} b'_H \\ b'_V \end{pmatrix} = \frac{b_H + b_V}{2} \begin{pmatrix} 1 \\ 1 \end{pmatrix} + \frac{a_H - a_V}{2} \begin{pmatrix} 1 \\ -1 \end{pmatrix} . \tag{27}$$

Similarly, for an R/L-basis PBS we have

$$\begin{pmatrix} a'_H \\ a'_V \end{pmatrix} = \frac{a_H - \mathrm{i}a_V}{2} \begin{pmatrix} 1 \\ \mathrm{i} \end{pmatrix} + \frac{b_H + \mathrm{i}b_V}{2} \begin{pmatrix} 1 \\ -\mathrm{i} \end{pmatrix} \tag{28}$$

and

$$\begin{pmatrix} b'_H \\ b'_V \end{pmatrix} = \frac{b_H - \mathrm{i}b_V}{2} \begin{pmatrix} 1 \\ \mathrm{i} \end{pmatrix} + \frac{a_H + \mathrm{i}a_V}{2} \begin{pmatrix} 1 \\ -\mathrm{i} \end{pmatrix} . \tag{29}$$

B. Light Sources

VQOL provides three different sources of light that are commonly available: a light-emitting diode for thermal light, a laser for coherent light, and a parametric downconversion source for entangled light. All sources are assumed to have a coherence time of Δt, so an independent random realization of the ZPF is drawn every time step. VQOL does not provide single-photon sources or indeed sources for any Fock states other than the vacuum. Since these three light sources produce Gaussian states, they may be modeled classically by an equivalent Gaussian random vector, as described below.

A **light-emitting diode (LED)** is a source of incoherent thermal light. In VQOL, an LED is treated as a monochromatic light source, with a wavelength of $\lambda = 496.61\,\mathrm{nm}$ (603.68 THz) that is perfectly collimated, appearing as a beam of constant width. An LED is specified by the parameter `power`, in Watts, with a default value of $4\,\mathrm{mW}$. The Jones vector of an LED is $\sqrt{\sigma^2 + \sigma_0^2}\,\boldsymbol{z}$, where $\boldsymbol{z}$ is a standard complex Gaussian random vector and $\sigma \geq 0$ specifies the total power

$$P = (\sigma^2 + \sigma_0^2)\frac{\hbar\omega}{\Delta t} , \tag{30}$$

where Δt is the length of each time step and $\omega = 2\pi c/\lambda$. Note that the `power` parameter in VQOL is actually $P - P_0$, where $P_0 = \sigma_0^2 \hbar\omega/\Delta t = 2.0000 \times 10^{-13}\,\mathrm{W}$. This is done to ensure that the vacuum modes persist even with the `power` parameter set to zero.

A **laser (LAS)** in VQOL is a coherent monochromatic light source that is perfectly collimated. The Jones vector of a laser is of the form $\boldsymbol{\alpha} + \sigma_0 \boldsymbol{z}$, where $\boldsymbol{\alpha} = \alpha\,|\psi\rangle$, $\alpha = 10^5$ (in dimensionless units), and $|\psi\rangle$ is a normalized polarization vector. (Note that, although the use of "ket" notation is suggestive of a quantum state, here we use it solely to represent a normalized complex vector.) Lasers may be configured so that $|\psi\rangle$ takes one of the following six standard forms:

$$|H\rangle = \begin{pmatrix} 1 \\ 0 \end{pmatrix} , \qquad |V\rangle = \begin{pmatrix} 0 \\ 1 \end{pmatrix} \tag{31a}$$

$$|D\rangle = \frac{1}{\sqrt{2}} \begin{pmatrix} 1 \\ 1 \end{pmatrix} , \quad |A\rangle = \frac{1}{\sqrt{2}} \begin{pmatrix} 1 \\ -1 \end{pmatrix} \tag{31b}$$

$$|R\rangle = \frac{1}{\sqrt{2}} \begin{pmatrix} 1 \\ \mathrm{i} \end{pmatrix} , \quad |L\rangle = \frac{1}{\sqrt{2}} \begin{pmatrix} 1 \\ -\mathrm{i} \end{pmatrix} \tag{31c}$$

The wavelength of a laser is the same as that of an LED, with the same default power as well. However, lasers will exhibit far less variability in both amplitude and polarization unless strongly attenuated. The total power, P, is related to the average photon number, $\|\boldsymbol{\alpha}\|^2 = |\alpha_H|^2 + |\alpha_V|^2$, by

$$P = \left(\|\boldsymbol{\alpha}\|^2 + \sigma_0^2\right) \frac{\hbar\omega}{\Delta t} . \tag{32}$$

For the default `power` setting of $4\,\mathrm{mW}$ we have $\|\boldsymbol{\alpha}\|^2 = 10^{10}$, which corresponds to an average photon number of 10 billion per time segment Δt. Using a neutral density filter with a default optical density of $d = 10$, the average photon number drops to just one nominal photon per time segment. If the `power` parameter is set to zero, the total power reduces to that of the vacuum.

Interestingly, VQOL also offers the ability to classically simulate multi-modal squeezed light and, hence, entangled states. A dual-spatial-mode **entanglement source (ENT)** based on parametric downconversion is used as a notional source of entangled photons. Entanglement sources can be type-I or type-II and are parameterized by a squeezing strength parameter r and relative phase φ. The Jones vectors for an entanglement source are a direct translation of the Bogoliubov transformations, with the annihilation operators replaced by complex Gaussian random variables [5]. Since the multi-modal

Fig. 6. (Color online) Illustration of light sources in VQOL. Shown above are an LED (top), a laser (middle), and an entanglement source (bottom).

squeezed vacuum states are Gaussian, this provides a faithful representation of the joint statistical distribution.

In VQOL, the Jones vector for a type-I entanglement source is given by

$$\begin{pmatrix} a_H \\ a_V \\ b_H \\ b_V \end{pmatrix} = \sigma_0 \begin{pmatrix} z_{1H}\cosh r + z_{2H}^* \sinh r \\ z_{1V}\cosh r + \mathrm{e}^{\mathrm{i}\varphi} z_{2V}^* \sinh r \\ z_{2H}\cosh r + z_{1H}^* \sinh r \\ z_{2V}\cosh r + \mathrm{e}^{\mathrm{i}\varphi} z_{1V}^* \sinh r \end{pmatrix} , \tag{33}$$

where $z_{1H}, z_{1V}, z_{2H}, z_{2V}$ are independent standard complex Gaussian random variables. The Jones vectors $\boldsymbol{a} = (a_H, a_V)^{\mathsf{T}}$ and $\boldsymbol{b} = (b_H, b_V)^{\mathsf{T}}$ correspond to the two spatial modes and notionally represent the two entangled photons. For a type-II entanglement source we have the Jones vector

$$\begin{pmatrix} a_H \\ a_V \\ b_H \\ b_V \end{pmatrix} = \sigma_0 \begin{pmatrix} z_{1H}\cosh r + z_{2V}^* \sinh r \\ z_{1V}\cosh r + \mathrm{e}^{\mathrm{i}\varphi} z_{2H}^* \sinh r \\ z_{2H}\cosh r + \mathrm{e}^{\mathrm{i}\varphi} z_{1V}^* \sinh r \\ z_{2V}\cosh r + z_{1H}^* \sinh r \end{pmatrix} . \tag{34}$$

The VQOL entanglement source provides a statistical representation of macroscopic Bell states [19]. For small r, the type-I entanglement source may be used to approximate the entangled state

$$|\Phi\rangle = \frac{|HH\rangle + \mathrm{e}^{\mathrm{i}\varphi}\,|VV\rangle}{\sqrt{2}} , \tag{35}$$

while for a type-II source it may be used to approximate the entangled state

$$|\Psi\rangle = \frac{|HV\rangle + \mathrm{e}^{\mathrm{i}\varphi}\,|VH\rangle}{\sqrt{2}} . \tag{36}$$

This correspondence may be made clearer by examining correlated measurements. The default settings for an entanglement source are $r = 1$ and either $\varphi = 0°$, for a type-I source, or $\varphi = 180°$, for a type-II source.

An entanglement source has a fixed orientation, but the directions of the two outgoing beams can be configured with the parameter `directions`. By default, this parameter is set to LR, indicating that $\boldsymbol{a}$ travels to the left and $\boldsymbol{b}$ travels to the right. Other options are LU (left, up), LD (left, down), UR (up, right), DR (down, right), and UD (up, down).

C. Measurement Devices

VQOL offers two types of measuring devices, a **power meter (PM)** and a **detector (D)**. The power meter acts as a photodetector operating in linear mode, so it reports the total incident power at each time step (including contributions from the vacuum). Power meters register power from any direction, so they have no orientation. If more than one light source illuminates a given power meter, it reports the largest power among the illuminating sources.

Given a Jones vector $\boldsymbol{a} = (a_H, a_V)^{\mathsf{T}}$, the power meter will report the value

$$P = \sqrt{|a_H|^2 + |a_V|^2}\,\frac{\hbar\omega}{\Delta t} , \tag{37}$$

where ω and Δt are defined as before. Note that P represents the slowly varying, time-averaged power of the wave. Fluctuations on a time scale below Δt are not seen. Power levels are displayed with up to three significant figures but recorded to within $1\,\mathrm{nW}$ of precision. In particular, power levels below $1\,\mathrm{nW}$ will be displayed and recorded as zero. If the user highlights the power meter while the simulation is running, it will display the current and time averaged power in the configuration window.

A detector in VQOL acts as a photodetector operating in Geiger mode. It will produce a detection count (or "click") when the amplitude of either the horizontal or vertical component falls above a given threshold $\gamma \geq 0$. Detectors have an effective dead time of Δt, as there can be at most one detection per time step. A detector is parameterized by its dark count rate (DCR), measured in counts per second. The DCR is related to the dark count probability, δ, via the formula $\mathrm{DCR} = \delta/\Delta t$. By default, DCR is set to 1000 counts per second (or 1/ms), corresponding to a dark count probability of $\delta = 0.001$. The detection threshold for a given dark count probability δ is found from Eqn. (13) to be

$$\gamma = \sigma_0 \sqrt{-\log\left(1 - \sqrt{1-\delta}\right)} . \tag{38}$$

For DCR = 1/ms, this takes the default value of $\gamma = 1.95$. The user may set the DCR value for each detector separately.

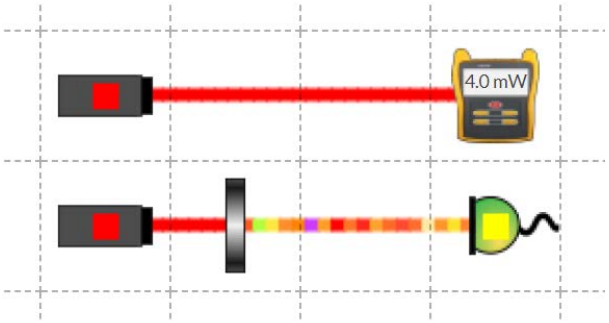

Fig. 7. (Color online) Illustration of measurement devices in VQOL. Shown above are a power meter (top) and single-photon detector (bottom), along with two lasers and a neutral density filter (gray rectangle). The power meter reads $4.0\,\mathrm{mW}$, and the detector has just made a detection.

V. Selected Examples

In this section we consider two different examples (and a few subvariants) of experiments that can be performed in VQOL. We begin with measuring detection efficiency using either a laser or an entanglement source. Next, we consider the Born rule using a polarizer and weak coherent light from a laser and a neutral density filter. Several other experiments, not discussed here, are possible. For example, from the Born rule experiment one may perform quantum state tomography to infer the density matrix of a prepared state. One may also consider wave/particle duality in the context of a Mach-Zehnder interferometer, as was done in Ref. [6]. One may also examine the use of an entanglement source to demonstrate anti-correlation or violations of the Bell-CHSH inequality [20], [21], [22]. Finally, one may consider the use of a beam splitter to perform a partial Bell state analysis and use this to implement a quantum teleportation scheme [23], [24]. In the examples to follow, special emphasis will be placed on the role of data analysis and post-selection to connect measured data with theoretical predictions. All component settings are taken to be their default values unless stated otherwise.

A. Detection Efficiency

In Eqn. (14) we identified η as the nominal detection efficiency. Operationally, the efficiency of a single-photon detector is measured by counting detection events relative to some reference photon flux. We may implement this scheme in VQOL using a laser (LAS), neutral density filter (NDF), and single detector (D), as shown in Fig. 8). The known power, P, of the laser and optical density, d, of the NDF allow us to estimate the photon flux as $R = 10^{-d}P/(\hbar\omega) = 10^{-d}\|\boldsymbol{\alpha}\|^2/\Delta t$. If we measure for a time t and obtain N counts, the inferred detection efficiency is

$$\eta_L = \frac{N}{Rt} \, . \tag{39}$$

This experiment was implemented in VQOL and run for different values of d and dark count rates. In each case we used a default laser power of 4 mW and an experiment time of $t = 1$ s. The results are summarized in Fig. 9. We observe that η_L has a peak value of about 15% at $d = 9.3$ for the default setting of DCR = 1/ms. Higher dark count rates give larger peak efficiencies and at larger values of d. For much larger values of d, corresponding to lower incident photon fluxes, the inferred detection efficiency actually goes over unity and becomes invalid, as detections are now dominated by dark counts. Thus, in VQOL, the detection efficiency is not an intrinsic property of the detector but, rather, is dependent upon the context of the measurement process.

An alternative scheme for measuring detection efficiency uses an entanglement source with post-selection heralding. The modified experiment is shown in Fig. 10, where we have replaced the laser with an entanglement source (ENT), removed the NDF, and now use two detectors, D1 and D2. A detection on D1 is construed to herald the presence of a photon at D2. Let N_1 denote the number of counts for which

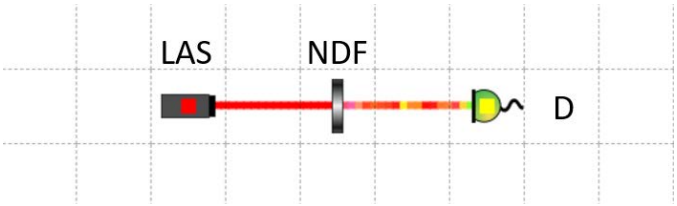

Fig. 8. (Color online) Experimental setup for measuring detection efficiency using a laser (LAS), neutral density filter (NDF) and single detector (D).

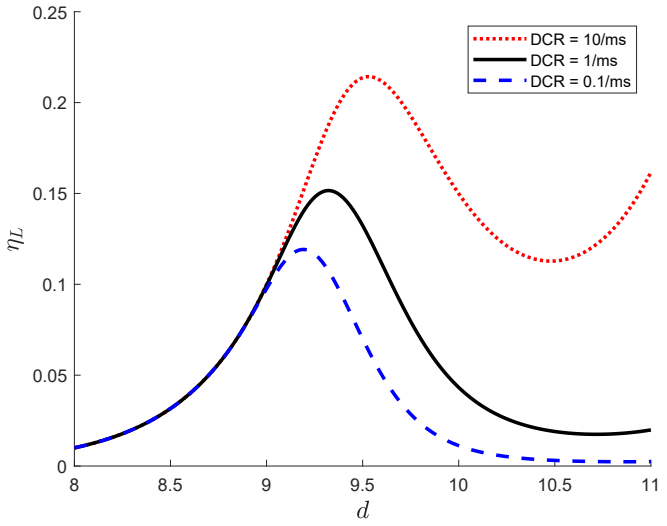

Fig. 9. (Color online) Plot of inferred efficiency η_L versus the optical density, d, for the NDF for different values of the dark count rate (DCR).

there is a detection on D1 but not D2. Similarly, let N_{12} denote the number of coincident counts on D1 and D2. The inferred detection efficiency may then be defined as

$$\eta_E = \frac{N_{12}}{N_1 + N_{12}} \, . \tag{40}$$

This experiment was also implemented in VQOL and run for different values of squeezing strength r and dark count rates. In contrast to η_L, we find that η_E approaches (but does not exceed) unity as r becomes large. There is also a dependence on the detection threshold, as parameterized by the DCR, that is similar to η_L but not as dramatic. Again, we find that the inferred detection efficiency is not an intrinsic property of the detector itself and may even appear arbitrarily close to unity under the right measurement conditions. This, of course, is merely an artificiality born of the amplification that results from a high squeezing strength. In real experiments this effect may be suppressed by detector saturation, which is not currently implemented in VQOL.

B. The Born Rule

The Born rule provides the fundamental connection between quantum theory and observations. Here we illustrate a simple experiment that may be performed in VQOL for studying the Born rule [4]. The experiment uses an attenuated laser and

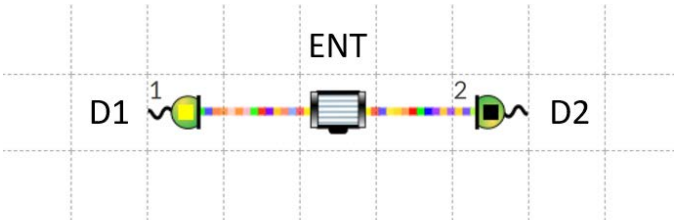

Fig. 10. (Color online) Experimental setup for measuring detection efficiency using an entanglement source (ENT) and two detectors (D1 and D2).

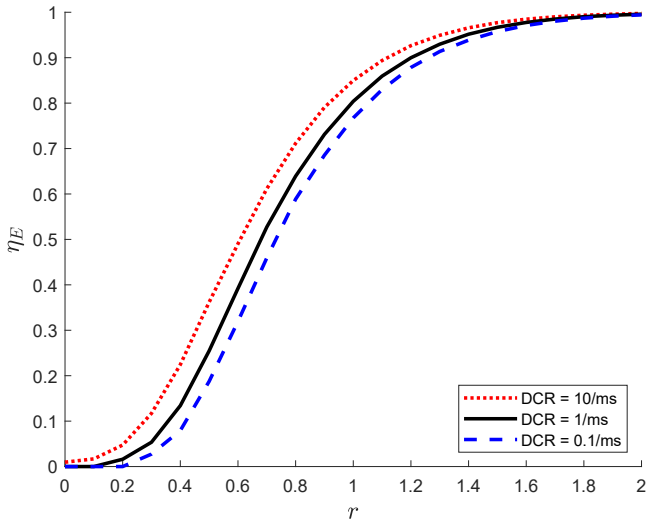

Fig. 11. (Color online) Plot of inferred efficiency η_E versus squeezing strength r for different values of the dark count rate (DCR).

polarizing filter with a single detector. One variation of this experiment, not discussed here, would be to replace the polarizer with a polarizing beam splitter and a pair of detectors. Another variation would be to use heralded detections with an entanglement source in place of the attenuated laser.

In this example we consider a simple experiment in which we prepare a laser (LAS) in the $|H\rangle$ polarization state and attenuate it using a neutral density filter (NDF), as shown in Fig. 12. A polarizer (P), set to an angle θ and phase ϕ, is placed before a detector (D). The polarizer has the effect of both attenuating the light and changing its polarization. The Jones vector of the light exiting the polarizer is given by

$$\begin{pmatrix} a_H \\ a_V \end{pmatrix} = 10^{-d/2}\alpha\cos\theta \begin{pmatrix} \cos\theta \\ \mathrm{e}^{\mathrm{i}\phi}\sin\theta \end{pmatrix} + \sigma_0 \begin{pmatrix} z_H \\ z_V \end{pmatrix} , \quad (41)$$

where $\alpha = 10^5$ is the default amplitude of the laser and $d = 10$ is the default optical density of the NDF. In accordance with Malus's law, the intensity varies as $\cos^2\theta$.

From the quantum perspective, we may view this experiment as the preparation of the $|H\rangle$ quantum state and subsequent measurement of the $|\psi\rangle$ state, where

$$|\psi\rangle = \begin{pmatrix} \cos\theta \\ \mathrm{e}^{\mathrm{i}\phi}\sin\theta \end{pmatrix} . \quad (42)$$

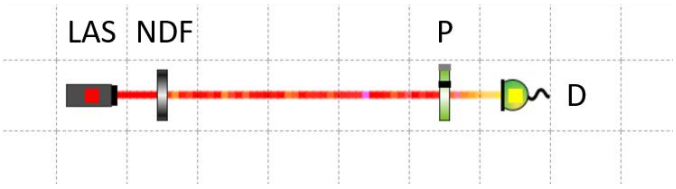

Fig. 12. (Color online) Experimental setup for the Born rule using a laser (LAS), neutral density filter (NDF), polarizer (P), and detector (D).

For a single photon, the Born rule predicts that the probability of a detection is $|\langle\psi|H\rangle|^2 = \cos^2\theta$. Although VQOL does not have a single-photon source, the laser and NDF provide a weak coherent state that may serve as a suitable approximation. If the optical density d is large, then only the single-photon and vacuum components of the coherent state will be significant.

In Fig. 13 we have shown the detection counts for a one-second experiment using a dark count rate of 100/ms for which we varied the polarizer angle θ while keeping $\phi = 0°$ fixed. The results are qualitatively similar to those of Malus's law, though we note that the number of counts at $\theta = 90°$ is not zero, due to the presence of dark counts.

The connection to probabilities is more subtle. The probability of an event is generally estimated as the ratio of the number of occurrences of the event to the number of trials. Experimentally, we measure the former, but the latter is unknown. (Of course, in VQOL we actually *do* know the number of trials, 10^6 in this case, but this is a detail hidden in the implementation and not something experimentally available.) A common strategy used by experimentalists is to subtract the dark counts, estimated here by the minimum number of counts, and rescale by the new maximum number of counts. Other strategies, such as fitting to a parametric curve, work similarly. Although this is common practice, it is important to understand that there is no "correct" strategy for associating counts with probabilities and that all such strategies incorporate some modeling assumptions.

In this example we have taken a rather large dark count rate. Lower dark count rates entail higher detection thresholds, for which the approximation of Eqn. (11) may therefore fail to hold, exhibiting deviations from the single-photon prediction. A similar effect is observed if d is too small and, hence, the laser too bright. Although good agreement can be found with high attenuation and low dark counts, the rate of detections in this regime may be quite low. The example we have shown here works well for a series of short, 1-ms experiments that can be run quickly and give good agreement under standard normalization.

VI. Discussion

We have illustrated a few examples of experiments in VQOL exhibiting characteristically quantum phenomena. In most cases, agreement between VQOL and the corresponding ideal quantum predictions is only approximate. This is due, in part, to our restriction to using only Gaussian states of light, such as coherent laser light or entangled squeezed light, which

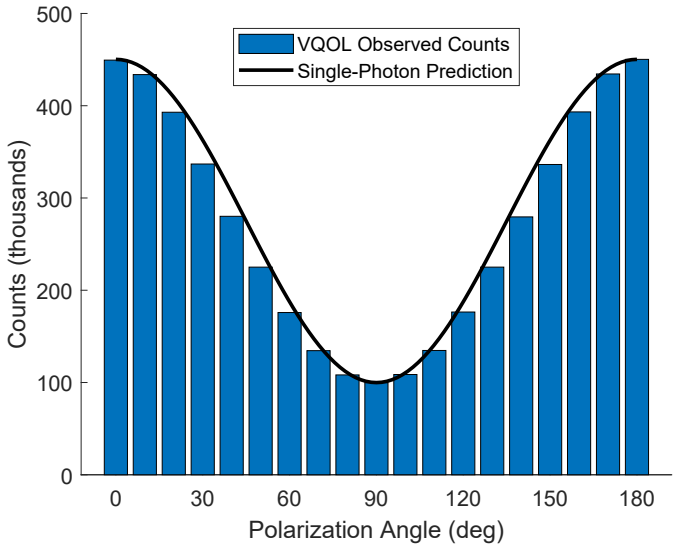

Fig. 13. (Color online) Detector counts (in thousands) versus the polarization angle θ (in degrees) for a DCR of 100/ms. The blue bars are measured results, while the black curve is the Born rule prediction for an ideal single-photon source.

contain contributions from vacuum modes as well as higher photon-number states. It is also due, in part, to our treatment of detectors as simple amplitude threshold crossing devices. Departures from ideal behavior can occur when the light source is too weak, in which case vacuum contributions may dominate, or when the light source is too strong, in which case multi-photon components may dominate. Similarly, different detection thresholds can provide varying levels of agreement. Thresholds that are too high will result is small sample sizes or necessitate long experiment runs; those that are too low may suffer from an excess of dark counts. The best agreement will depend on the experiment and the method of analysis but will usually be for intermediate values. In the examples discussed we have tried to identify parameter regimes that provide a good compromise between these competing factors.

We have also highlighted the important role of data analysis is comparing experimental observations to theoretical predictions. Quantum mechanics is fundamentally a theory of probabilities, and the meaning and estimation of these probabilities depends critically on the context and interpretation of the experiment. Although in principle one has access to the true underlying number of random trials in VQOL, we have emphasized how data analysis in real experiments must be performed without this information. In many cases, this leads to the necessity of performing post-selection on particular outcomes, such as the use of heralding to approximate single-photon sources or the use of coincident detections in performing quantum correlation experiments. Even in the absence of post-selection, renormalization may be required to obtain probabilities from raw counts. Furthermore, the removal of dark counts and "accidental" coincidences, both of which are common data analysis techniques, may also be required. The seemingly mundane process of comparing raw observations to theoretical predictions can be a critical step in understanding and interpreting quantum theory.

The restriction to 1-μs time bins is an artificiality intended to represent the typical dead time of an avalanche photodiode as well as the coherence times of the light sources. Common photodetection timing devices have a sampling resolution of about 1 ns, although timing jitter below 10 ps can be resolved [25]. This restriction makes VQOL ill suited for experiments focusing on high-resolution timing with small, nonzero time delays. Likewise, the subtle effects of detector afterpulsing and saturation are also ignored [26]. The choice of using a 1-μs coherence time is an artificiality born of expediency. At the beginning of each time step a new and independent random realization of the ZPF is drawn. At this time, any light incident upon a detector will either be such as to trigger a detection or not. If a detection is triggered, the detector remains dead until the next time step. Otherwise, the Jones vector remains unchanged (and hence cannot trigger a detection) until the next time step. In other words, the detectors are such that they do not accumulate energy over time but, rather, trigger immediately when adequate conditions are realized at the beginning of a time step. This is consistent with the rather short response times of avalanche photodiodes (typically less than a nanosecond) compared with their relatively long recovery times (typically around a microsecond).

VII. Conclusion

The Virtual Quantum Optics Laboratory (VQOL) is a versatile simulation tool that can be used to design and execute a wide array of experiments in classical and quantum optics. The simplicity of the user interface makes it a valuable classroom resource that can be used to introduce and explore quantum concepts. The novelty and sophistication of the underlying models also make it an excellent tool for exploratory theoretical research or as a complement to actual quantum optics experiments.

We have illustrated a few examples of experiments in VQOL exhibiting characteristically quantum phenomena. Many others are possible. Agreement with quantum theory is only approximate and depends critically on both the choice of parameter settings and the manner in which the data are post-selected and analyzed. In this regard, VQOL is very different from traditional simulators in that it is intended to more closely match observations than theory. Despite its simplicity, we believe VQOL can be a powerful tool for learning and understanding key quantum phenomena.

Acknowledgments

This work was supported in part by Applied Research Laboratories, The University of Texas at Austin (ARL:UT), the National Science Foundation (NSF), under Grant No. 1842086, and the Office of Naval Research (ONR), under Grant Nos. N00014-18-1-2233 and N00014-17-1-2107.

REFERENCES

[1] R. Müller and H. Wiesner, "Teaching quantum mechanics on an introductory level," *American Journal of Physics*, vol. **70**, p. 200, 2002.

[2] R. Scholz, S. Wessnigk, and K.-A. Weber, "A classical to quantum transition via key experiments," *European Journal of Physics*, vol. **41**, p. 055304, 2020.

[3] S. Bartlett, T. Rudolph, and R. Spekkens, "Reconstruction of Gaussian quantum mechanics from Liouville mechanics with an epistemic restriction," *Physical Review A*, vol. **86**, p. 012103, 2012.

[4] B. La Cour and M. Williamson, "Emergence of the Born rule in qunatum optics," *Quantum*, vol. **4**, p. 350, 2020.

[5] B. La Cour and T. Yudichak, "Entanglement and impropriety," *Quantum Studies: Mathematics and Foundations*, 2021.

[6] ——, "Classical model of a delayed-choice quantum eraser," *Physical Review A*, vol. **103**, p. 062213, 2021.

[7] G. Tóth, "QUBIT4MATLAB V3.0: A program package for quantum information science and quantum optics for MATLAB," *Computer Physics Communications*, vol. **179**, p. 430, 2008.

[8] J. Johansson, P. Nation, and F. Nori, "QuTiP 2: A Python framework for the dynamics of open quantum systems," *Computer Physics Communications*, vol. **184**, p. 1234, 2013.

[9] Z. Seskir *et al.*, "Quantum games and interactive tools for quantum technologies outreach and education," https://arxiv.org/abs/2202.07756.

[10] N. Killoran, J. Izaac, N. Quesada, V. Bergholm, M. Amy, and C. Weedbrook, "Strawberry Fields: A software platform for photonic quantum computing," *Quantum*, vol. **3**, p. 129, 2019.

[11] "QuantumLab," retrieved January 10, 2021, from https://www.quantumlab.nat.fau.de/english/index.html.

[12] "Quantum Lab," retrieved January 10, 2021, from https://quantumflytrap.com.

[13] "The Quantum Game," retrieved January 10, 2021, from http://play.quantumgame.io.

[14] K. Cahill and R. Glauber, "Density operators and quasiprobability distributions," *Physical Review*, vol. **177**, p. 1882, 1969.

[15] J. Marcum, "Table of Q functions," Rand Corporation, Santa Monica, CA, Tech. Rep. U.S. Air Force RAND Research Memorandum RM-339-PR, 1 January 1950.

[16] R. Jones, "A new calculus for the treatment of optical systems I. Description and discussion of the calculus," *Journal of the Optical Society of America*, vol. **31**, p. 488, 1941.

[17] H. Hurvitz and R. Jones, "A new calculus for the treatment of optical systems," *Journal of the Optical Society of America*, vol. **31**, p. 493, 1941.

[18] J. Clauser and M. Horne, "Experimental consequences of objective local theories," *Physical Review D*, vol. **10**, p. 526, 1974.

[19] T. Iskhakov, M. Chekhova, G. Rytikov, and G. Leuchs, "Macroscopic pure state of light free of polarization noise," *Physical Review Letters*, vol. **106**, p. 113602, 2011.

[20] P. Grangier, G. Roger, and A. Aspect, "Experimental evidence for a photon anticorrelation effect on a beam splitter: A new light on single-photon interferences," *Europhysics Letters*, vol. **1**, p. 173, 1986.

[21] J. Bell, "On the Einstein Podolsky Rosen paradox," *Physics Physique Fizika*, vol. **1**, p. 195, 1964.

[22] J. Clauser, H. Horne, A. Shimony, and R. Holt, "Proposed experiment to test local hidden-variable theories," *Physical Review Letters*, vol. **23**, p. 880, 1969.

[23] C. Bennett, G. Brassard, C. Crépeau, R. Jozsa, A. Peres, and W. Wootters, "Teleporting an unknown quantum state via dual classical and Einstein-Podolsky-Rosen channels," *Physical Review Letters*, vol. **70**, p. 1895, 1993.

[24] D. Bouwmeester, J.-W. Pan, K. Mattle, M. Eibl, H. Weinfurter, and A. Zeilinger, "Experimental quantum teleportation," *Nature*, vol. **390**, p. 575, 1997.

[25] I. Zadeh *et al.*, "Efficient single-photon detection with 7.7 ps time resolution for photon-correlation measurements," *ACS Photonics*, vol. **7**, p. 1780, 2020.

[26] M. Eisaman, J. Fan, A. Migdall, and S. Polyakov, "Invited review article: Single-photon sources and detectors," *Review of Scientific Instruments*, vol. **82**, p. 071101, 2011.